



Article

Experimental Study on Seismic Response of Underground Tunnel–Soil–Piled Structure Interaction Using Shaking Table in Loose Sand

SeyedSaeid Ekraminia ¹, Masoud Hajjalilue Bonab ¹ , Saba Ghassemi ¹ and Reza Derakhshani ^{2,*} 

¹ Department of Civil Engineering, University of Tabriz, Tabriz 5166616471, Iran; saba.ghassemi.1994@gmail.com (S.G.)

² Department of Earth Sciences, Utrecht University, 3584 CS Utrecht, The Netherlands

* Correspondence: r.derakhshani@uu.nl

Abstract: The seismic response of structures can have a significant impact on adjacent structures' response. Although several numerical studies have been applied in the field of tunnel–soil–pile interaction systems, there is a lack of experimental research specifically focused on the effects of this interaction on tunnel cross-section deformation and the existence of structure on encircling soil response. In this study, shaking table tests were conducted to examine the seismic response of a tunnel and the surrounding soil when an eight-story structure with piles was located in the vicinity of the tunnel. Four series of physical models were analyzed, including free-field soil (S), tunnel–soil (TS), soil–piled structure (SP), and tunnel–soil–piled structure (TSP), under sinusoidal vibration at three frequencies on loose sand. According to the results, the tunnel significantly impacts the surrounding soil response during seismic excitation with reduced acceleration at the tunnel invert and increased acceleration at the tunnel crown. In the TSP model, applied frequency affects the recorded acceleration amplitude at the tunnel invert. Although acceleration amplitude decreases at 3 Hz frequency excitation compared to the free field model, 8 Hz excitation resulted in bigger values in tunnel invert. Displacements are higher at the tunnel crown, indicating tunnel-induced soil deformation and maximum shear strain concentrated near the tunnel crown. The tunnel cross-section exhibited oval shape changes, with higher forces on the tunnel crown in the presence of piles.

Keywords: tunnel–soil–piled structure interaction; shaking table test; seismic response; pile foundation; bending moment; loose sand



Citation: Ekraminia, S.; Hajjalilue Bonab, M.; Ghassemi, S.; Derakhshani, R. Experimental Study on Seismic Response of Underground Tunnel–Soil–Piled Structure Interaction Using Shaking Table in Loose Sand. *Buildings* **2023**, *13*, 2482. <https://doi.org/10.3390/buildings13102482>

Academic Editor: Yong Tan

Received: 16 August 2023

Revised: 21 September 2023

Accepted: 26 September 2023

Published: 29 September 2023



Copyright: © 2023 by the authors. Licensee MDPI, Basel, Switzerland. This article is an open access article distributed under the terms and conditions of the Creative Commons Attribution (CC BY) license (<https://creativecommons.org/licenses/by/4.0/>).

1. Introduction

Considering the impact of shallow tunnels on the propagation of seismic waves and the seismic response of the surrounding soil, piled structures can have an impact on this issue via their reflective, seismic, or inertial effects. The uncertainty of this interaction's beneficial or destructive effect has sparked debates, which is the subject of this study.

Numerous studies have been conducted to thoroughly analyze the effects of past earthquakes, including the Kobe, Hyogoken-Nambu, and Wenchuan earthquakes, on the behavior of tunnels [1–4]. Despite tunnels' known resilience to seismic activity [5], previous research on severely damaged underground structures has established that it is crucial to recognize the underground structures' vulnerability to structural damage during powerful ground motions [6–8]. During the Hyogoken-Nambu earthquake in Japan in 1995, nearly all utility tunnels were impacted by seismic activity. The damage experienced by each tunnel was directly related to its proximity to the epicenter, with those closer experiencing more significant damage. However, some other researchers indicated that shallow tunnels are at a higher risk of earthquake damage during the same period than deep tunnels [7]. In fact, approximately 60% of tunnels constructed at a depth of less than 50 m have endured severe deformations. Also, SBD-K-medoids-based long-term settlement analysis of shield tunnel

was conducted and demonstrated that artificial intelligence is an emerging technology that can be used to analyze the seismic response of underground tunnel–soil-piled structure interaction problem and exemplified the rationality and engineering practice value of the study’s approach and offered a new method for analyzing the long-term settlement of shield tunnels [9].

Furthermore, the outcomes of recent post-earthquake investigations into the effects of earthquakes have revealed that the inertia force exerted by structures during an earthquake can have a significant reflection on the foundation and its sub-surface structures. This interaction can lead to soil deformation due to the building’s vibration [10]. Thus, it is crucial to accurately assess piled structures’ performance in soil–structure interaction systems for designing safe structures in earthquake-prone areas. For instance, research on soil–pile–structure interaction using a shaking table summarizes that this interaction significantly increases the period for the oscillator attached to a free-head pile [11]. Contradictory results have arisen from research on seismic soil–structure interaction; while some studies indicate that it can prolong the system period and enhance damping [12,13], others suggest that it could lead to a greater amplitude of accelerations, larger displacements, and catastrophic failures [14–17], which depends on the respective dynamic characteristics of the soil and structure and adaptability of the soil–structure interaction system, both of which can be true to some extent.

Considering the mentioned research, the interaction between the surface structure, piles, and tunnels can be complex for designing tunnels in urban areas due to their proximity. This can affect the seismic response of tunnels, which is generally determined by the seismic load in the free field. For instance, numerical analyses of the development of tunneling influence zones for adjacent pile foundations discovered that the influence domain could be identified based on factors such as ground condition, pile geometry, tunnel construction method, and evaluated criteria [18]. Ptilakis et al. [19] numerically investigated the impact of single and multiple adjacent surface structures on the seismic response of underground tunnels. The findings revealed that the surrounding soil’s shear wave and pressure fields were altered by the presence of surface structures, which affected the tunnel’s seismic response. It was also observed that this impact was more pronounced for tunnels that were buried at shallower depths. Azadi and Hosseini [20] studied the seismic wave’s effect on the interaction between double tunnels and surface structure and illustrated that the type of structure and earthquake frequency components have a significant impact on the horizontal displacement and bending moment responses of both surface and embedded structures. An experimental study on tunnel interaction with soil and structures on dense sand uncovered that the presence of a tunnel weakened the rigidity of the model, leading to an amplified seismic response in the surrounding soil. Also, the type of seismic wave had a considerable impact on the system’s response [21]. Moreover, Franza et al. [22] conducted a simplified elastic analysis of tunnel-piled structure interaction and declared that tunnel excavations induce flexural deformations beneath piles.

Comprehensive research on tunnel–soil interaction, tunneling effects, soil–structure interaction, and the effect of piles on the seismic response of soil was conducted using various numerical methods, centrifuge, shaking table, and field tests [23–30]. Although there is a lack of experimental investigation regarding the combined effects of these structures, it is vital to study the effect of existing structures on tunnels and their seismic response. Given that most of the experiments performed in this field have been applied on dense sand or clay (due to the difficulty of making low-density specimens and the non-reproducibility of experiments on a sample), further research is needed to study the behavior of tunnels, structures, and piles in loose sand. The present study experimentally investigated the tunnel–soil-piled structure interaction, focusing on tunnel behavior. In twelve shaking table tests conducted on loose sand using a laminar box, sinusoidal loading was applied, with the acceleration value kept constant while the frequency was changed. This adjustment in frequency was made because previous research has shown its significant impact on the

model response. It should be noted that the investigation did not examine the influence of pile axial forces on the tunnel's response.

2. Experimental Setup

2.1. Shaking Table Properties and Soil Container

Physical modeling investigations can be carried out to reproduce the conditions of a particular problem on a smaller scale than the real scale. These investigations are conducted in the laboratory under 1 g (using a shaking table) or N_g (using a centrifuge) conditions. This research used shaking table tests to conduct four series of physical modeling tests on the scaled system of tunnels, soil, and piles connected to the eight-story structure.

With a rectangular steel test platform and dimensions of 3 m \times 2 m, the shaking table of Tabriz University has 6 ton capacity and one directional ground motion. Its range of displacement is ± 100 mm. Seismic operation is designed at 0.1–20 Hz range, and the input movement is applied to the test platform by a horizontal hydraulic actuator (Figure 1).

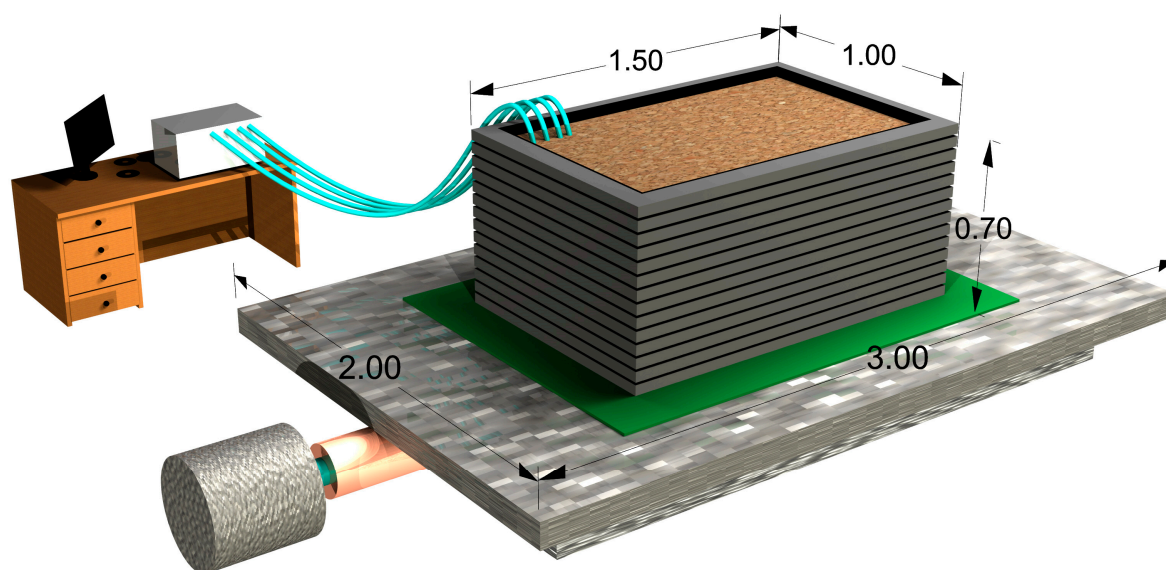


Figure 1. The 3D figure of the shaking table and the research model on it (units: meter).

Choosing a suitable container plays a vital role in physical modeling research. A layered container was selected to simulate the free field condition better and measure soil displacements at different levels by LVDT. The box was made of stacked aluminum rings in a rectangular shape; each has an external dimension of 1.5 m \times 1 m and an internal dimension of 1.37 m \times 0.86 m. The total height of the box is 80 cm, which was filled up to 65 cm for experiments, and then the extra rings were removed to prevent inertial errors. Using a plastic membrane prevented the soil from spilling out and entering between the bearings (Figure 1). Analyzing the peak acceleration response of soil at various depths illustrated that the reflection of seismic waves at the box's boundary can be neglected.

Uniformly graded sand (Gumtapeh sand) was chosen, and its characteristics are given in Table 1. Moreover, using the air pluviation method, which has been used in similar studies [31], improved reproducibility, prevented human errors in sample-making, and resulted in almost uniform samples.

Table 1. Basic properties of Gumtapeh sand.

Soil Property	Gs (gr/cm ³)	D10 (mm)	D30 (mm)	D60 (mm)	Cc	Cu	Y _d Min (gr/cm ³)	Y _d Max (gr/cm ³)	Unified Category
Magnitude	2.66	0.21	0.3	0.43	0.996	2.047	1.49	1.72	SP

2.2. Simulation Ratio and Model Structures

According to the available facilities, the most appropriate method was a geometric similarity in physical modeling. This research used 1 g shaking table scaling laws to simulate the test conditions [32]. A geometric scale coefficient of 45 was chosen based on similarity rules, equipment capacity, and laminar box size, and scaling relations are given in Table 2.

Table 2. Scale factors of physical modeling.

Item	Scaling Factor (Prototype/Model)	Values in This Study
Length	λ	45
Density of saturated soil	λ_p	$1.8/1.56 = 1.154$
Strain of soil	$\lambda_\varepsilon = \lambda / [(Vs)_p / (Vs)_m]^2$	$45 / [375/80]^2 = 2.048$
Time	$\lambda_t = (\lambda \lambda_\varepsilon)^{0.5}$	9.6
Frequency	$\lambda_f = (1/\lambda_t)$	0.104
Total stress	$\lambda \lambda_p$	51.9
Acceleration	1	1

The characteristics of tunnel and structure models were obtained and reported in Table 3 via the numerical modeling and application of λ to geometric parameters. In Table 3, the columns' heights were reported for each story. However, it should be noted that the columns were constructed as one piece along all stories. It is important to note that the results are significantly affected by frequency. Therefore, ensuring that the natural frequency of the modeled structure matches the natural frequency of an actual 8-story building is imperative. The numerical modeling results indicate that the natural frequency of an actual 8-story structure was 1.025 Hz. By applying the frequency coefficient (λ_f), the natural frequency of the modeled structure was determined to be 9.85 Hz. However, due to construction limitations, the actual natural frequency of the modeled structure was slightly altered to 9.94 Hz.

Table 3. The material information and properties of the tunnel, structure, and piles.

Item	Dimension (cm)	Material
Tunnel	length = 80 external diameter = 20 thickness = 0.15	Aluminum
Structure	stories area = 25×25 stories thickness = 0.2 column section area = 0.1×4 column height = 7.1	Steel (ST-37)
Pile	section area = 0.2×3 height = 30	Aluminum

2.3. Tests Processing and Sample Making

The study conducted experiments on physical models to investigate the effects of different conditions under sinusoidal loads. Four series of physical models were constructed, each with varying conditions but subjected to the same acceleration and different frequencies. The presence of piles and the limited understanding of soil–tunnel performance in loose sand motivated the choice of loose sand. Because of modifications in soil density and residual moments that remained on the tunnel model, samples were prepared and studied for each test separately. The first model (S) focused solely on examining the soil in free field conditions. The air pluviation method with a relative density (D_r) of 40% was employed to fill the box with soil, reaching a height of 65 cm. In the second one, the tunnel–soil model (TS), the box was initially filled with soil up to a height of 10 cm. Subsequently, a tunnel

was placed into the box, and the filling process was continued accordingly (Figure 2). The filling operation was deliberately paused above the tunnel during each cycle to prevent any disturbance. To account for the influence of the distance between underground and surface structures, as well as the buried depth of the underground structure, the tunnel and piles were strategically positioned in close proximity to each other. This arrangement aimed to assess the seismic response of the system comprehensively, considering the aforementioned factors. The third model, known as the soil–pile (SP) model, followed the same process as the first model. After moving the box on the shaking table, the piled structure was placed on top of the soil sample. Similarly, the fourth model, referred to as the tunnel–soil–piled structure (TSP), was prepared in the same manner as the second model. Once transferred to the table, the piled structure was added to the model (Figure 2). Figure 3 illustrates the three types of physical models employed in the study.



Figure 2. The tunnel and structure model in their location.

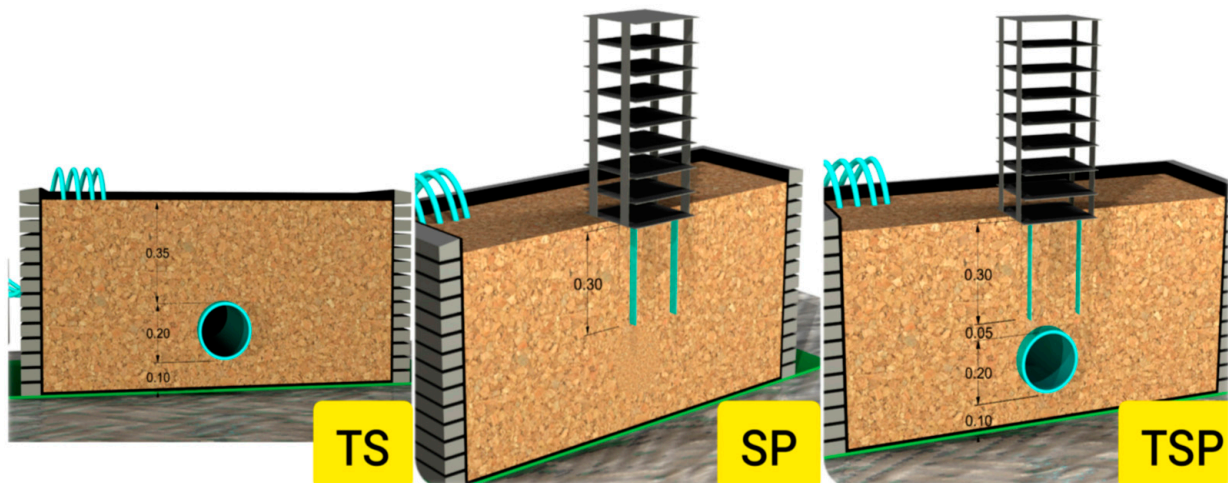


Figure 3. TS, SP, and TSP models in shaking table tests (units: meter).

Six accelerometers were positioned in the same direction at different depths to record the effects of one-dimensional input vibrations. The recorded data were collected using a data logger. Furthermore, eight strain gauges were installed on the tunnel cover to measure the strain and bending moment experienced by the tunnel lining during vibration. In addition, five LVDTs were utilized to measure the displacement of the laminar box at the same levels as the accelerometers (Figure 4).

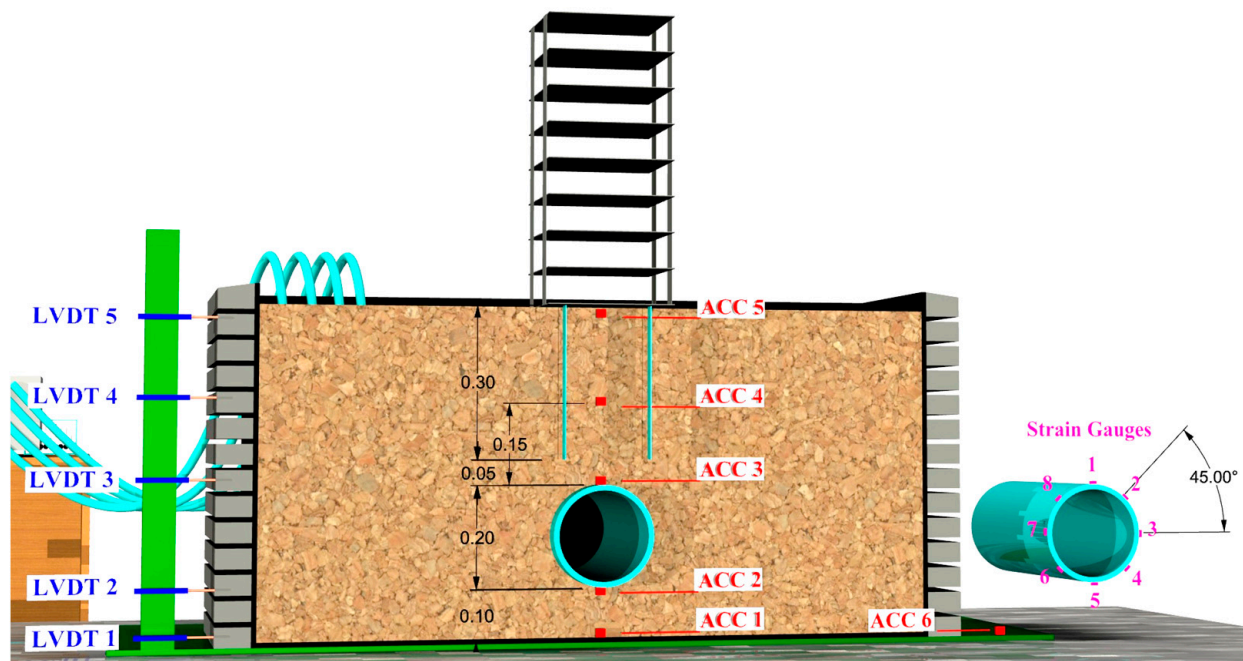


Figure 4. The shaking table test layout with locations of sensors (units: meter).

Twelve shaking table experiments were conducted at a constant acceleration of 0.5 g (sinusoidal loading) and frequencies of 3, 5, and 8 Hz (Table 4). As frequency dramatically affects the results [20], other parameters were kept as constant as possible throughout the study.

Table 4. Setup of shaking table tests.

Test ID	Model	Inputted Ground Acceleration (g)	Frequency (Hz)	Displacement Range of Shaking Table (mm)
S-3	Soil	0.5	3	±13.8
S-5	Soil	0.5	5	±4.9
S-8	Soil	0.5	8	±1.9
TS-3	tunnel–soil	0.5	3	±13.8
TS-5	tunnel–soil	0.5	5	±4.9
TS-8	tunnel–soil	0.5	8	±1.9
SP-3	soil–pile	0.5	3	±13.8
SP-5	soil–pile	0.5	5	±4.9
SP-8	soil–pile	0.5	8	±1.9
TSP-3	tunnel–soil–pile	0.5	3	±13.8
TSP-5	tunnel–soil–pile	0.5	5	±4.9
TSP-8	tunnel–soil–pile	0.5	8	±1.9

3. Results and Discussion

The residual strain was observed on the tunnel structure during the low-frequency vibrations. However, this strain was eliminated after evacuating the soil. Despite the presence of residual strain, both the tunnel and structure models did not experience structural failure during the tests. In order to ensure accurate measurements, the strain gauges were calibrated correctly and checked for each test. Although the structure did not collapse in any of the experiments, asymmetric subsidence was observed during the SP-3 test.

A white noise test was conducted in the SP model to estimate and compare the dynamic responses of the structure. The structure's natural frequency was also calculated using acceleration data collected at various levels of the structure, with six accelerometers. After

analyzing the numerical modeling result (9.94 Hz) for the structure's natural frequency and comparing it to the value obtained from the white noise test (10.68 Hz), the verification of the model was confirmed. Although there was a minor discrepancy between the measured and numerical values due to construction limits and errors, it was negligible. The free field dynamic test revealed that the natural frequency of the soil model was 16.8 Hz, indicating that resonance could be prevented.

3.1. Study on Structure–Soil–Structure Interaction

In all the reports, the S model acceleration results were used as a basis for comparison, and any increase or decrease in the recorded acceleration amplitude reported was compared to the S model. As shown in Figure 5, the ACC1 results for all four models are close to each other, and no significant change is observed.

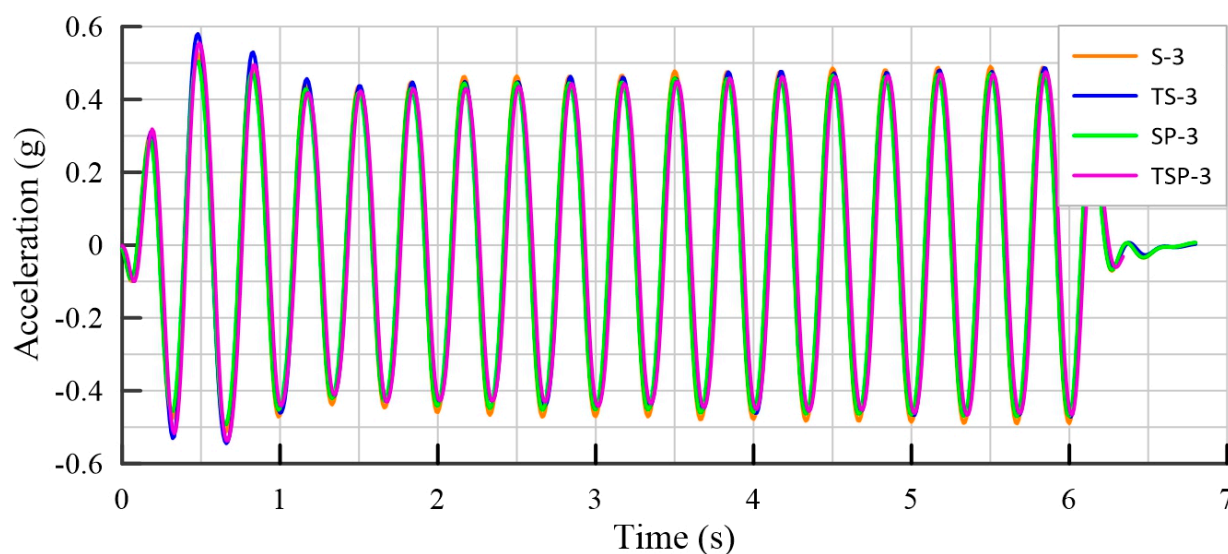


Figure 5. ACC1 results in 0.5 g acceleration and 3 Hz frequency in four models.

Numerous methods have been proposed in previous studies to study maximum displacement. In these investigations, the maximum displacement of each LVDT was selected for comparison. For each test, five specific times were identified, with one of the LVDTs experiencing the highest displacement at each of these moments. It is worth noting that different LVDTs could record varying displacement values during these moments. Each diagram illustrates how the entire model deforms when one of the LVDTs reaches its maximum displacement. To normalize the data, these displacement values were divided by the maximum displacement value of the shaking table, as extracted from ACC6 data. As a result, for each test, five separate graphs were generated, each focusing on the moment when one of the LVDTs recorded the highest displacement. For easier comparison, Figure 6 presents a graph for each test where LVDT 1 records the greatest displacement. This type of chart is known as an “RDS chart”, which stands for “Recorded Displacement by LVDT1-5 divided by the Maximum Displacement obtained from ACC6 results”. According to Figure 6, all four models (S, TS, SP, and TSP) experience a similar maximum displacement at the ACC1 depth. However, the deformation mode varies at lower depths between the different models. The TS model shows the highest displacement on the sample surface, indicating that the tunnel causes the surface to move further during maximum bed movement. Despite what happens to the TS model, in the TSP model, the piled structure has effectively prevented surface deformation. Although a massive, piled structure can limit significant displacements, it may be deleterious for lightweight structures with shallow foundations [33].

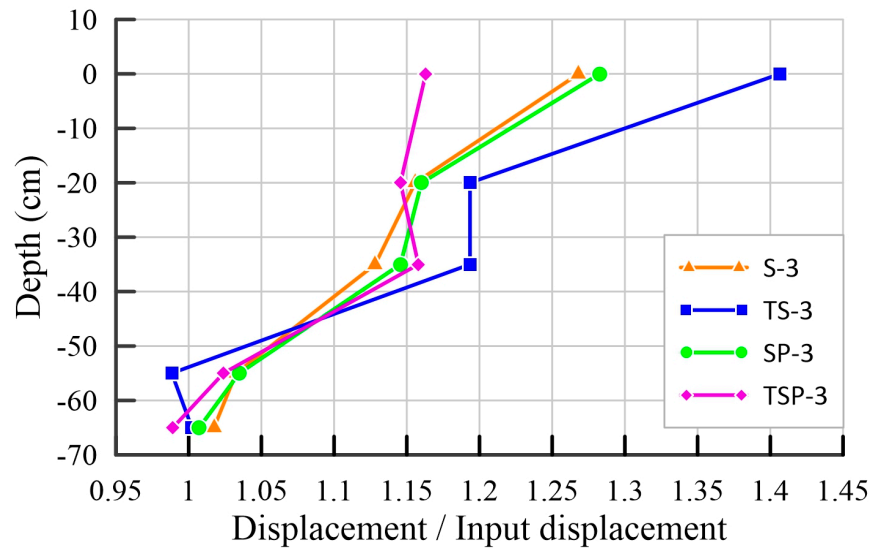


Figure 6. RDSD of four tests when LVDT1 has maximum displacement value for each model at 3 Hz frequency.

A glance at the ACC2 results (Figure 7) reveals the tunnel effect on the seismic response of the models. The tunnel in the TS model at all frequencies has diminished the recorded acceleration amplitude in the vicinity of tunnel invert compared to the S model, which has not been affected by the input frequency. For more details, the acceleration diagram of the vibration’s final second is shown in Figure 7a–c.

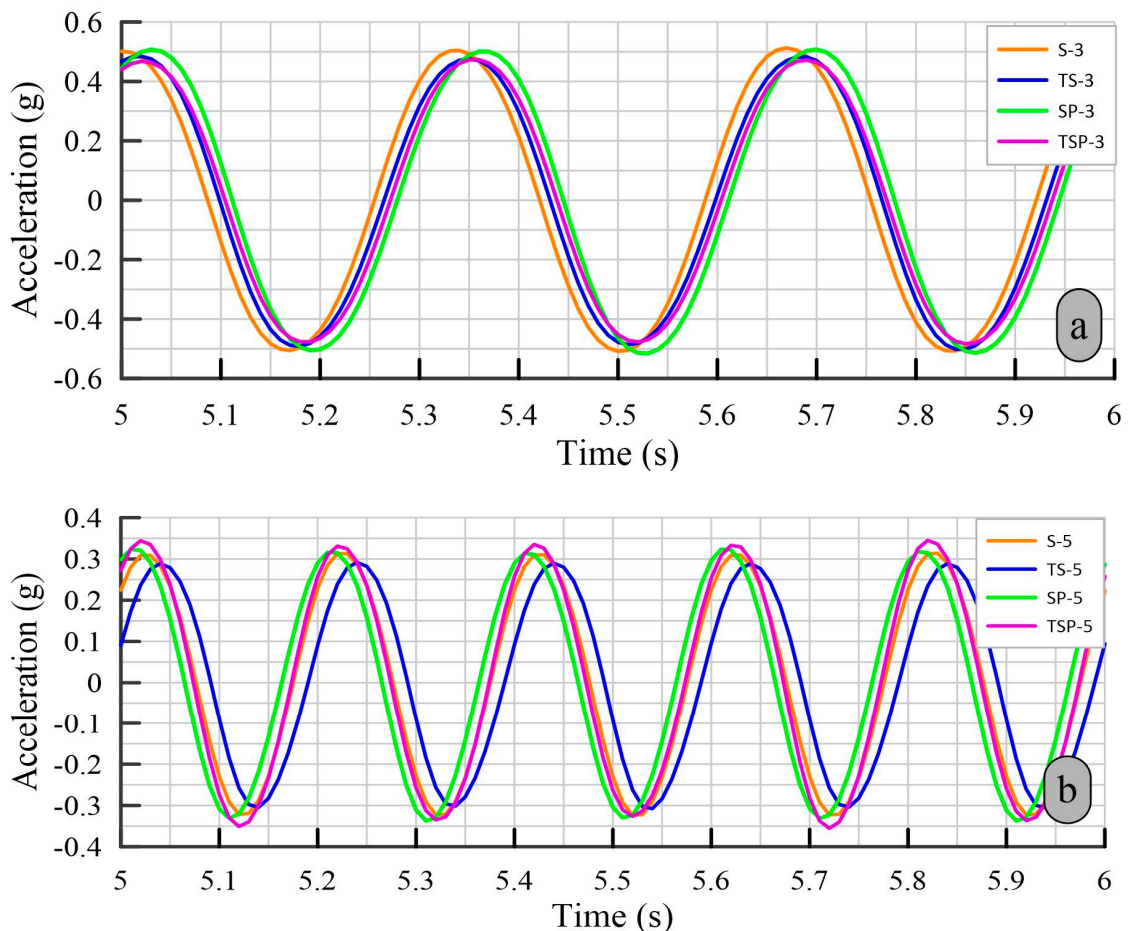


Figure 7. Cont.

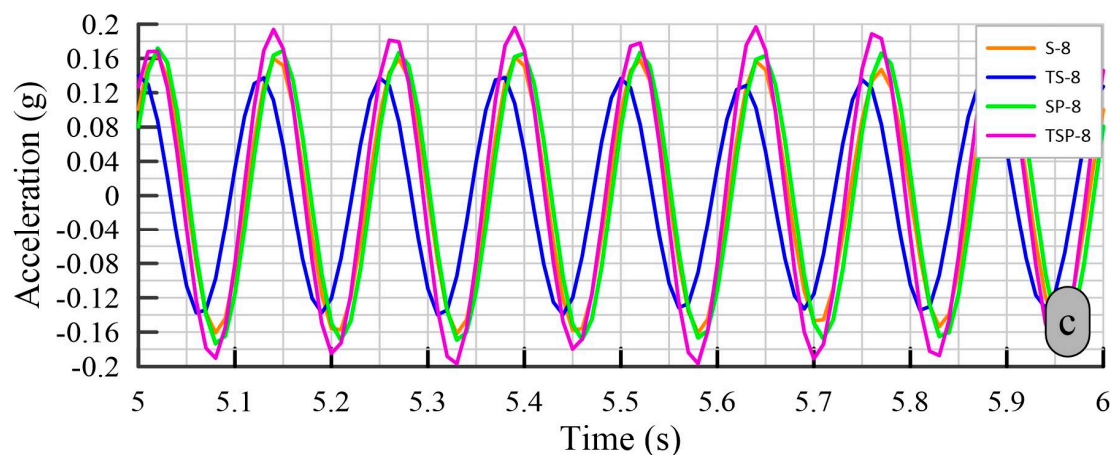


Figure 7. ACC2 final second acceleration diagrams recorded for four models at a frequency of (a) 3 Hz, (b) 5 Hz, and (c) 8 Hz.

The presence of the tunnel reduces the acceleration amplitude by at least 10% across all frequencies. This reduction becomes more pronounced as the frequency increases. Ding et al. [34] previously estimated that rectangular-shaped tunnels can experience a decrease in peak acceleration ranging from 0.4 g to 0.8 g under the tunnel. SP model's diagram indicates no notable alterations, although different behavior is observed with the simultaneous presence of piled structure and tunnel (TSP model). The acceleration amplitude of the tunnel invert exhibits a reduction at a frequency of 3 Hz; however, it increases as the frequency is raised to 5 Hz and further to 8 Hz. This indicates that the applied frequency significantly influences the results of the tunnel invert in the TSP models, and Figure 7b,c evidently demonstrate this effect. Previous numerical studies have demonstrated that the presence of surface structures can lessen the seismic response of tunnels. This finding is consistent with the results obtained from the S-3 and TSP-3 experiments, confirming the surface structure's mitigating effect on the tunnel's seismic response [35]. However, it was also observed that various types of earthquake waves have varying impacts on the response of an interaction system [21]. Additionally, the presence of piles near the tunnel can amplify this impact. Two models (TS and TSP) perform similarly at low frequencies.

Figure 8 presents a normalized RDSD diagram of the 3 Hz frequency tests when LVDT2 reaches maximum displacement. From the diagram, it is clear that both the TS and TSP models experience similar deformation patterns. Additionally, the displacement at a depth of -35 cm (tunnel crown) in the TS-3 experiment increases compared to the S model. This observation highlights the impact of the tunnel and piled structure on the displacements, particularly at the specified frequency of 3 Hz. Furthermore, a comparison between the TSP and TS results reveals the reduction of the effect of the tunnel at 3 Hz (Figure 8) and the amplifying effect at 5 Hz (Figure 9). It is noteworthy to mention the increased movement at the -35 cm and -20 cm depths (piles location) in the SP model. As expected, the relative deformation of the S and SP models remains close to each other within the range of -65 cm to -55 cm. However, an increase in displacement is observed at different depths in the SP model, indicating that the piles contribute to the linear deformation of the soil profile. Moreover, increasing the frequency causes higher soil displacement at the -55 cm depth in both the SP and TSP models compared to the free field soil model (S).

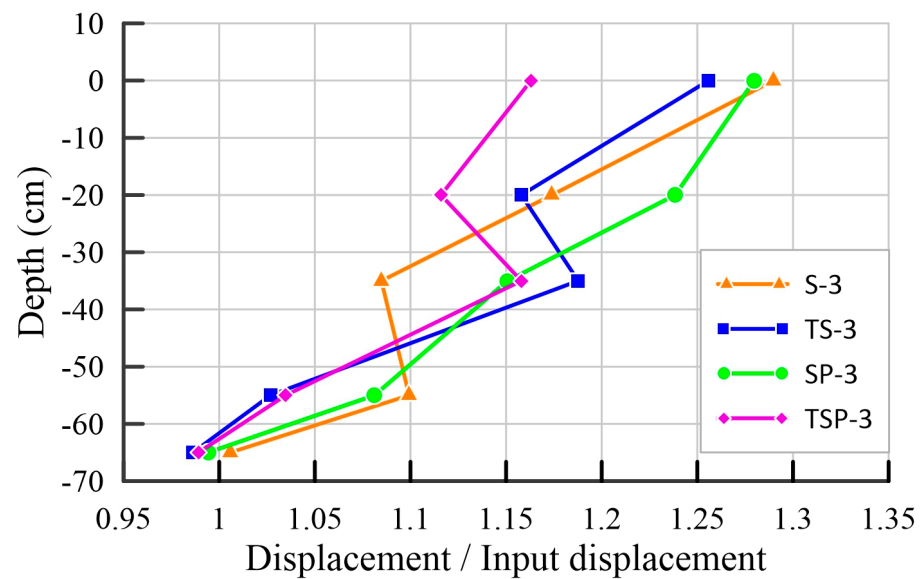


Figure 8. RDSD of four tests when LVDT2 has maximum displacement value for each model in 3 Hz frequency.

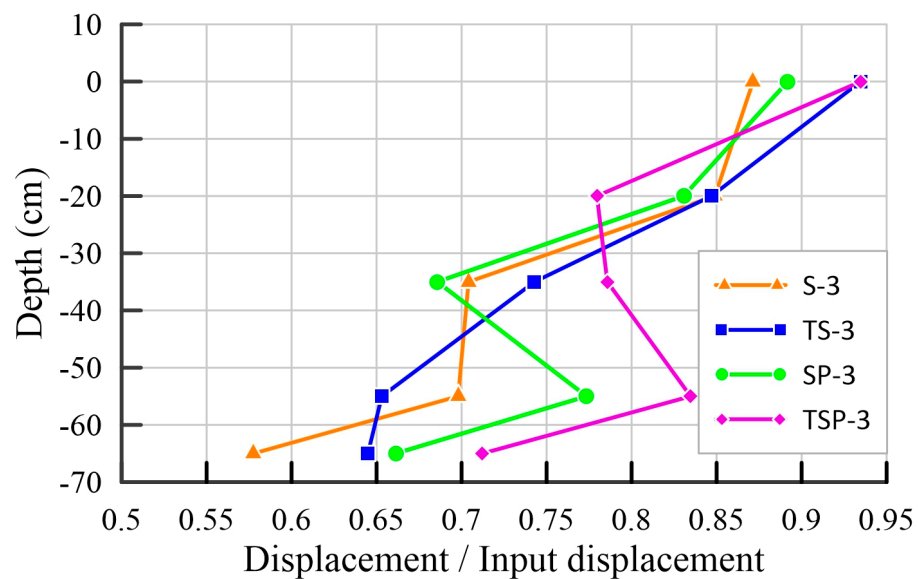


Figure 9. RDSD of four tests when LVDT2 has maximum displacement value for each model in 5 Hz frequency.

The data collected from ACC3 demonstrate an increase in acceleration amplitude across the three models compared to the S model (Figure 10). This observation highlights the fact that both the tunnel and piles contribute to an increase in acceleration amplitude at the top of the tunnel crown and the end of the piles. Notably, at a frequency of 3 Hz, the tunnel has the most significant influence on the results, with the largest recorded amplitude in this model. As the frequency increases to 5 Hz and subsequently 8 Hz, acceleration amplitude increases dramatically in the TSP model compared to the other models. To summarize, the coexistence of both the tunnel and piles has the most effect on the seismic response at higher frequencies, as demonstrated in Figure 10. This observation aligns with previous numerical investigations, such as the study conducted by Tsinidis [36]. The findings of the previous investigation highlighted a significant increase in the seismic response of the tunnel when a nearby building or structure is present. Additionally, the results obtained from ACC2 and ACC3 indicate that a lower buried depth leads to an

enormous acceleration amplification factor. This observation is consistent with earlier research by Hashash et al. [7], which confirms that underground structures experience a stronger seismic response when buried at shallower depths.

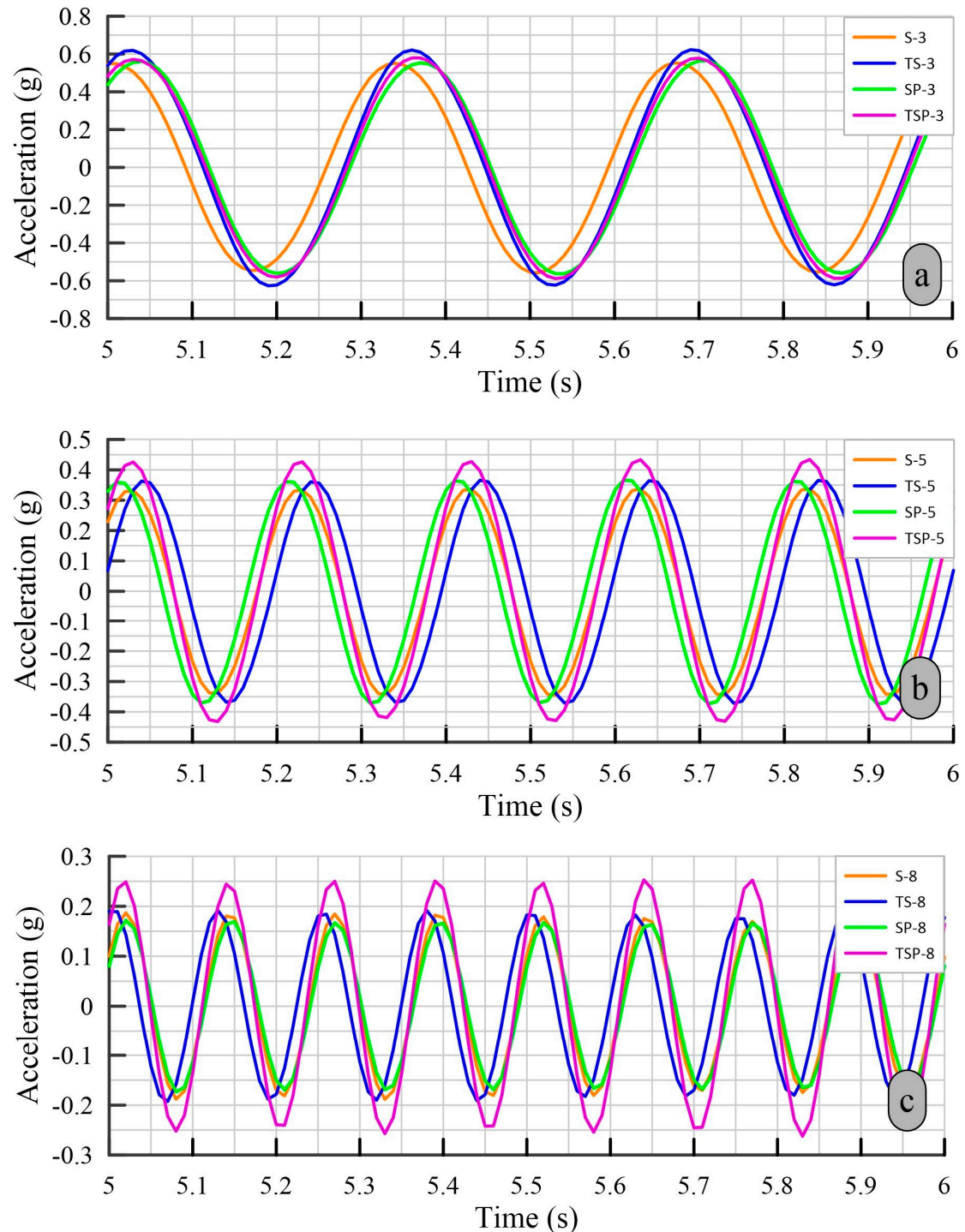


Figure 10. ACC3 final second acceleration diagram for four models at frequencies of (a) 3 Hz, (b) 5 Hz, and (c) 8 Hz.

The normalized RSDS graph obtained at the critical moment from LVDT3 highlights the impact of the TS model on the increased displacement at -35 cm depth. In contrast, tunnel invert experiences relatively minor displacement compared to other models. The highest shear strain occurs in this area and turns it into a critical region (Figure 11), and

there is a considerable difference between -55 and -35 cm depth displacement values in the TS model; by changing frequency to 8 Hz, TSP-8 experiences the most relative deformation in this range (Figure 12).

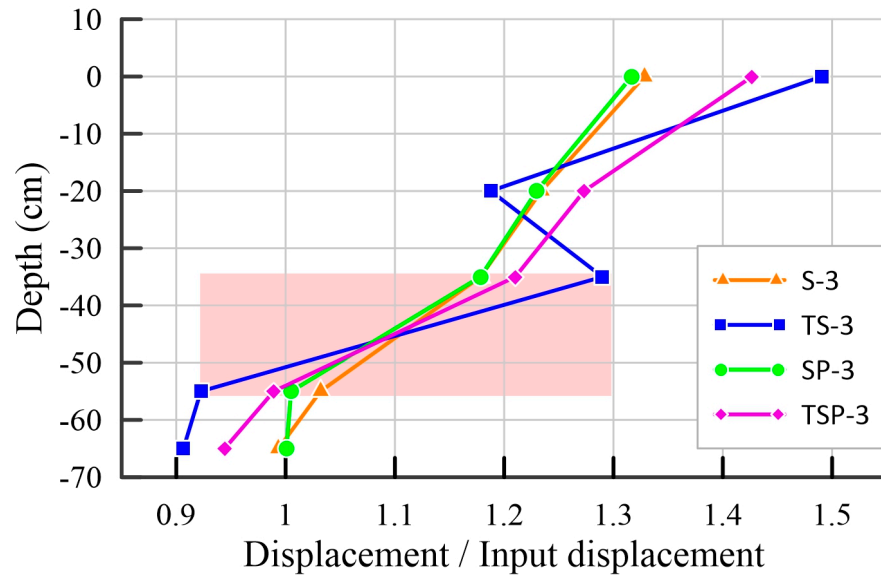


Figure 11. RDS of four tests when LVDT3 has maximum displacement value for each model at 3 Hz frequency.

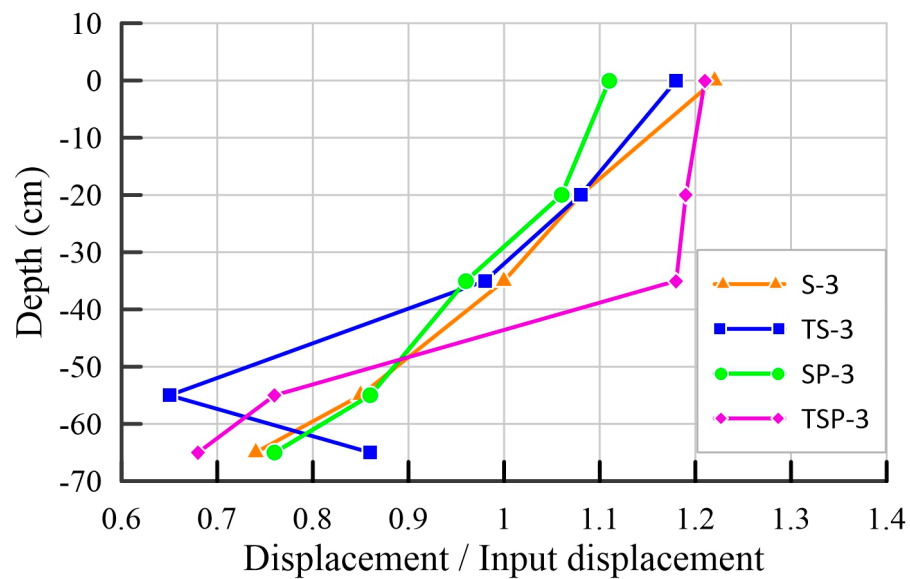


Figure 12. RDS of four tests when ACC3 has maximum displacement value for each model in 8 Hz frequency.

ACC4 and ACC5 results, plotted at 5 Hz in Figure 13, present an amplification in floor-to-surface acceleration transfer in all three models compared to the S model. The most significant impact is on the 8 Hz frequency and the TSP model, which increases the acceleration values by up to 30%.

Figure 14 depicts the amplification factor of ACC2, ACC3, ACC4, and ACC5 to provide a more transparent representation of the models' behavior. The amplification factor is defined as the ratio of the maximum acceleration recorded by different accelerometers to that of ACC1. To eliminate any initial errors, the first and second responses of all tests are disregarded.

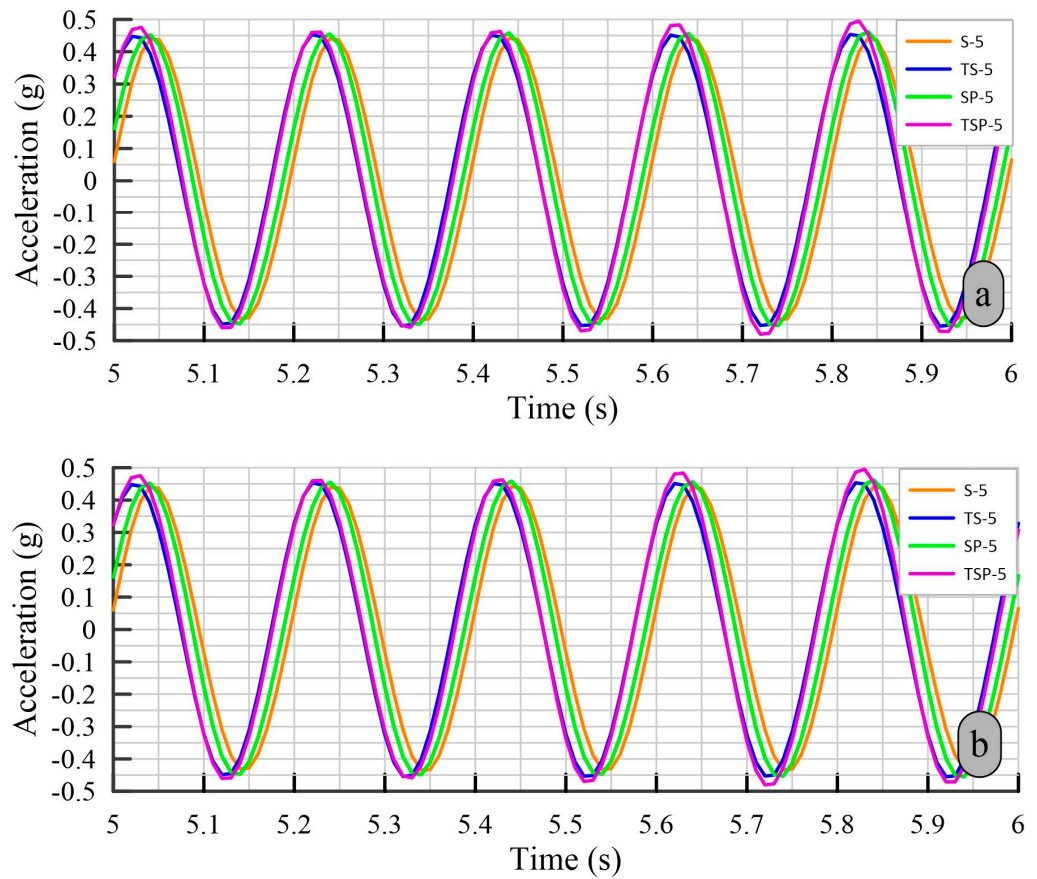


Figure 13. (a) ACC4 and (b) ACC5 final second acceleration diagram for four models at the frequency of 5 Hz.

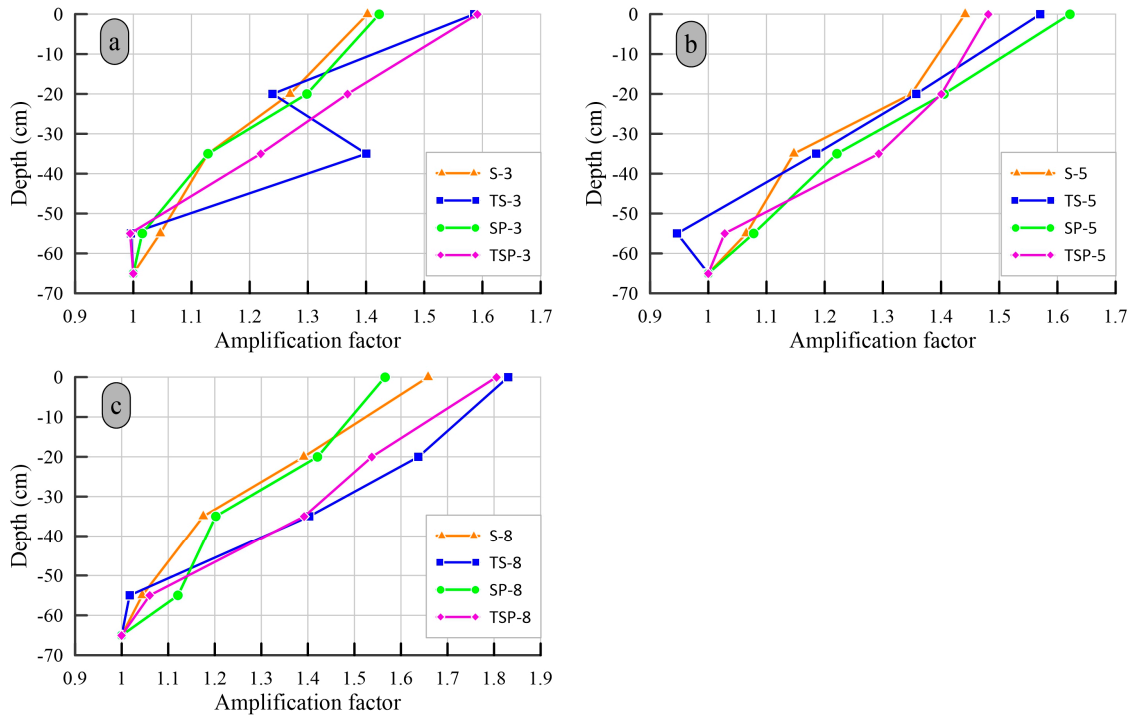


Figure 14. Amplification factors of ACC2 to 5 in all models for (a) 3 Hz, (b) 5 Hz, and (c) 8 Hz frequencies.

3.2. Investigating Impacts of Variables Soil Profile Strain

Zeghal and Elgamal [37] and Zeghal et al. [38] revealed that if the soil profile is considered a one-dimensional shear beam, shear stresses and shear strains of certain depths can be calculated using acceleration measurements of those depths. Therefore, by calculating the shear stress–strain during the excitation, the relevant hysteresis curves are extracted, and the parameters of shear modulus will be obtained from these curves.

This research uses a quasi-static analysis of the free field's seismic response related to the rock bed to measure stress and strain values. The used results are an approximation of the dynamic analysis performed for the one-dimensional wave propagation by Roeset [39] and Gazetas [40]. It is important to note that quasi-static analysis is valid for low excitation frequencies. Considering that the acceleration is measured discretely, assuming linear changes in acceleration with depth and using interpolation between acceleration measurements, the shear stress at depth z is calculated using the following equation [38]:

$$\tau_i(t) = \sum_{k=1}^{i-1} \rho \cdot \frac{\ddot{u}_k(t) + \ddot{u}_{k+1}(t)}{2} \cdot \Delta z_k \quad (i = 2, 3 \dots) \quad (1)$$

In Equation (1), τ is the shear stress, \ddot{u} is the acceleration, ρ is the density of the soil, and Δz_k is the distance between two consecutive accelerometers. Gazetas [40], by dynamic analysis of the equation for one-dimensional wave propagation, explained that if the changes of G with depth are assumed to be linear, the value of the shear strain can be calculated using the following equation:

$$\gamma_{(z)_i} = \frac{\left[(u_{i+1} - u_i) \left(\frac{Z_i - Z_{i-1}}{Z_{i-1} - Z_i} \right) + (u_i - u_{i-1}) \left(\frac{Z_{i+1} - Z_i}{Z_i - Z_{i-1}} \right) \right]}{(Z_{i+1} - Z_{i-1})} \quad (2)$$

In Equation (2), γ is the shear strain, u is the displacement, and z is the height. According to Equation (2), to obtain the shear strain at depth (i), the results of three consecutive accelerometers or LVDTs must be available. The stress and shear strain values are calculated using the results of accelerometers for three depths (ACC2, ACC3, and ACC4 locations).

At a depth of -55 cm, the shear strain values in the TS, SP, and TSP models declare a significant reduction compared to the S model at a frequency of 3 Hz, as depicted in Figure 15. Among the three models, the TS model demonstrates the most considerable reduction. The tunnel decreases shear strain values at this depth. Conversely, at a depth of -35 cm (tunnel crown), both the TS and SP models experience increased shear strain within the same stress range, as illustrated in Figure 16.

In the TSP model, a notable increase in shear strain is observed above the tunnel, indicating that the simultaneous presence of the tunnel and piled structure significantly elevates the shear strain value. This finding follows the numerical findings presented by Yu and Wang [35]. At the -20 cm depth, the presence of piles unexpectedly induces an increase in shear strain, which is evident in both the SP and TSP models (Figure 17). Notably, the largest increase in shear strain occurs in the vicinity of the tunnel crown in the TSP model, suggesting that this area can be identified as the critical shear zone. These results further corroborate the findings derived from the accelerometer diagrams.

To better understand the effect of frequency on the recorded strain, the 8 Hz frequency results are shown in Figures 18–20. The models experienced a different trend at a depth of -55 cm in all three models (TS, SP, and TSP), the shear strain increased, and the highest value was related to the TS model. At a depth of -20 cm, the SP model reduces the shear strain, and in stark contrast, the TS model increases the shear strain. A predictable performance from the TSP model is observed, and its values fluctuate in the SP and TS model outcomes range. Also, there is a markable difference between 3 Hz and 8 Hz frequency results.

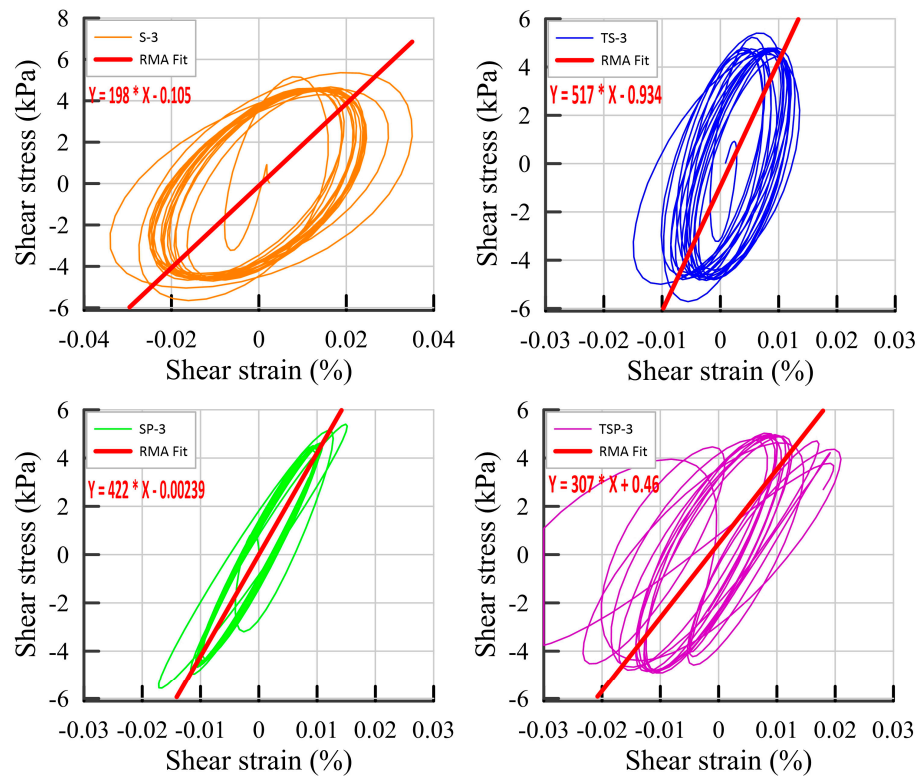


Figure 15. Shear stress–shear strain diagrams for four models at –55 cm depth at the frequency of 3 HZ.

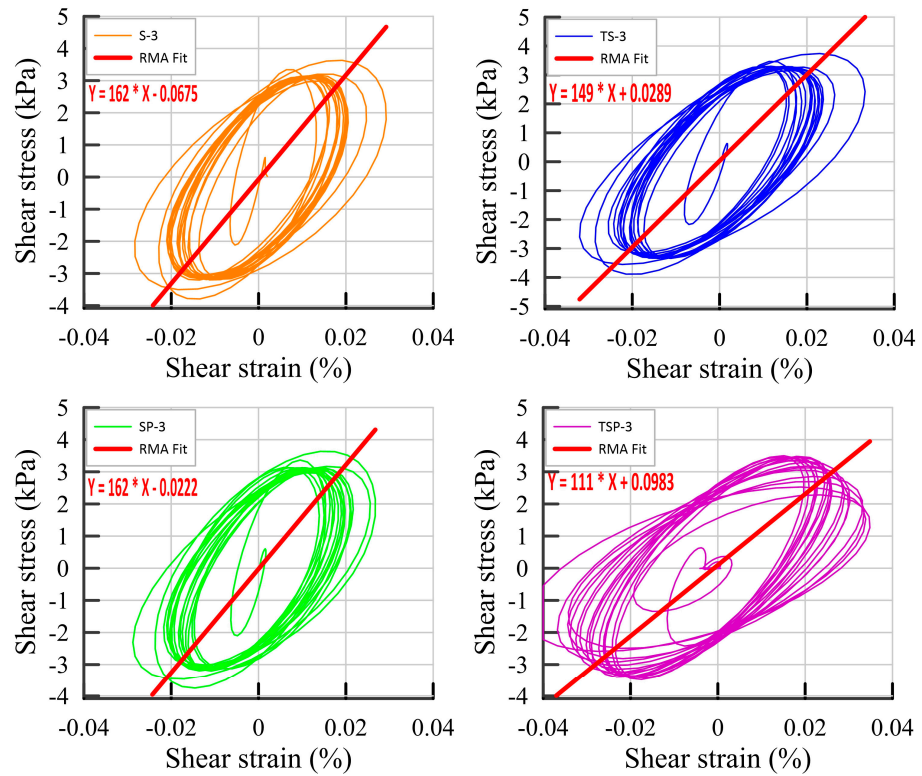


Figure 16. Shear stress–shear strain diagrams for four models at –35 cm depth at the frequency of 3 HZ.

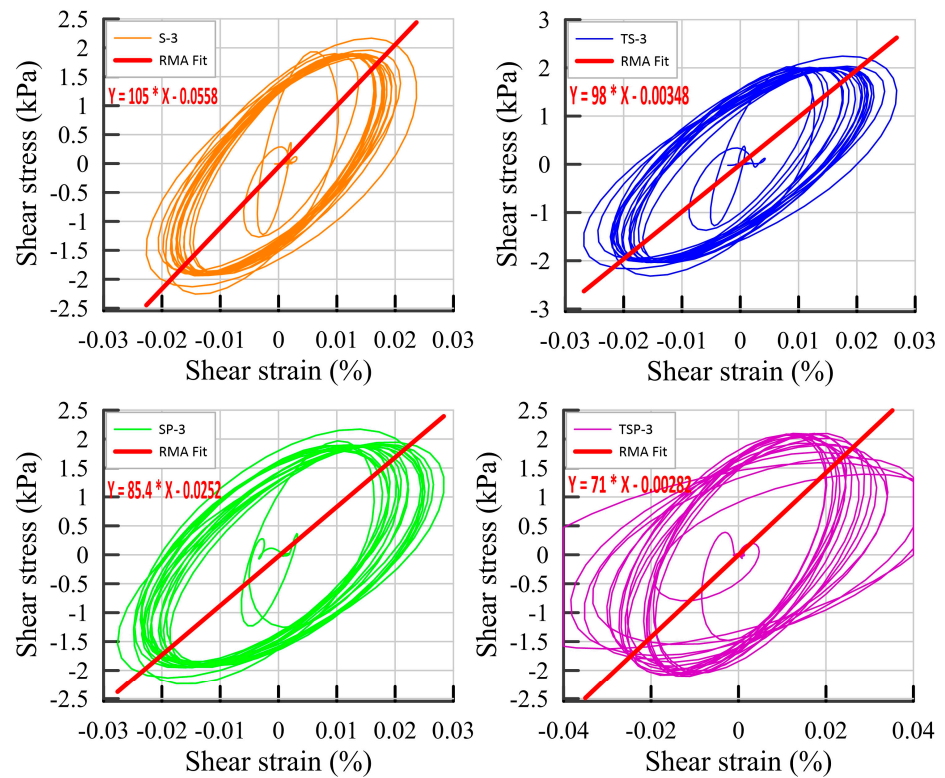


Figure 17. Shear stress–shear strain diagrams for four models at –20 cm depth at the frequency of 3 HZ.

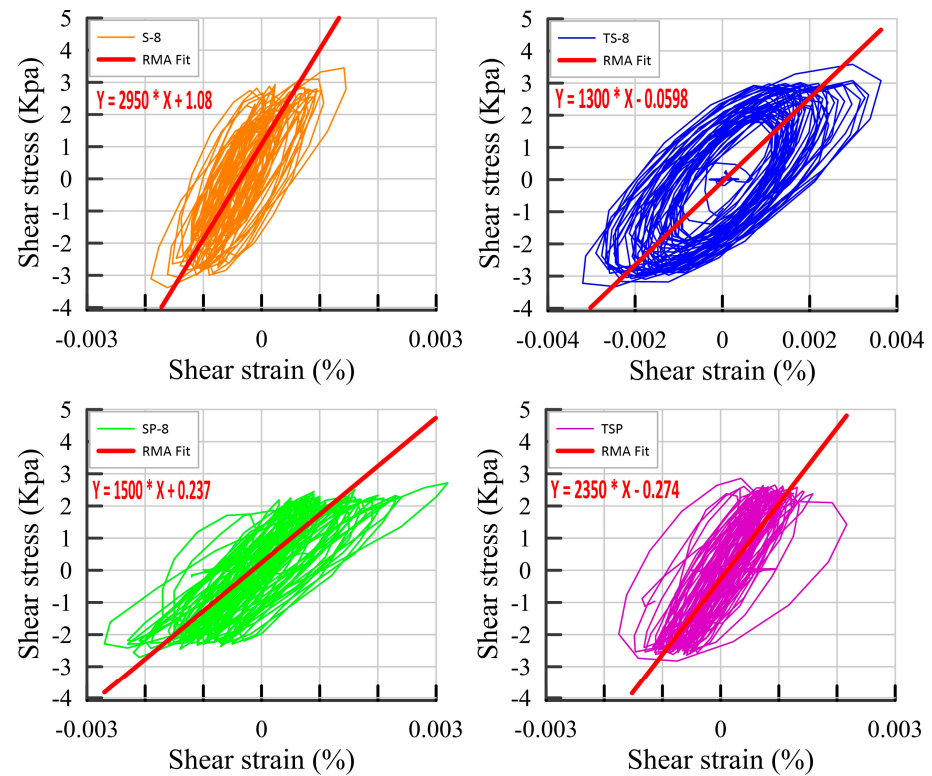


Figure 18. Shear stress–shear strain diagrams for four models at –55 cm depths at the frequency of 8 HZ.

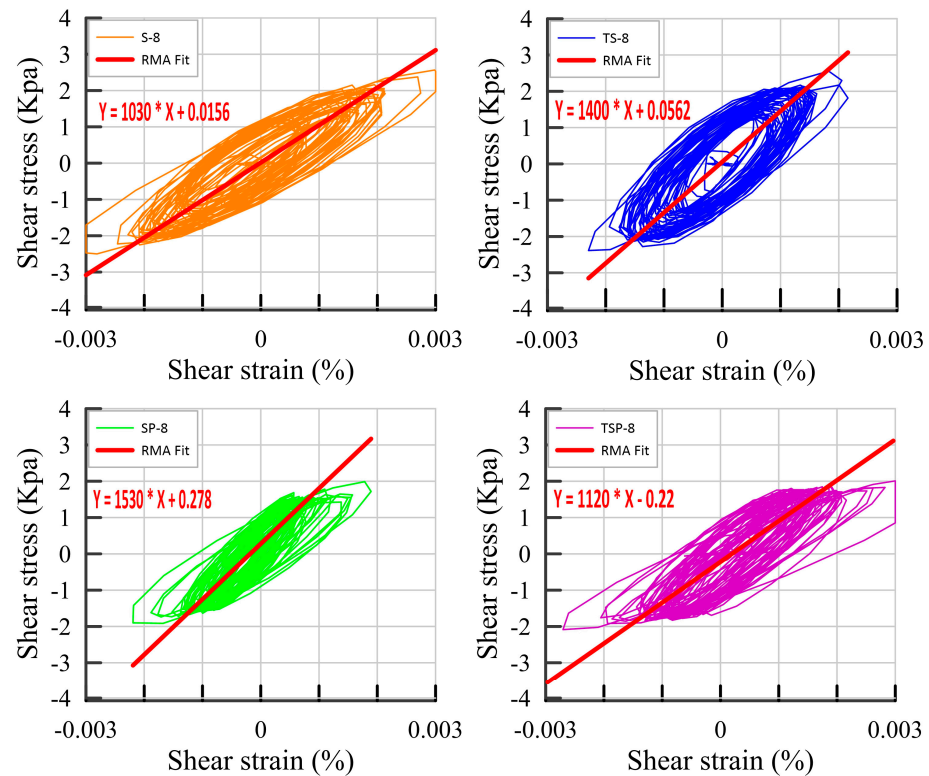


Figure 19. Shear stress–shear strain diagrams for four models at –35 cm depths at the frequency of 8 HZ.

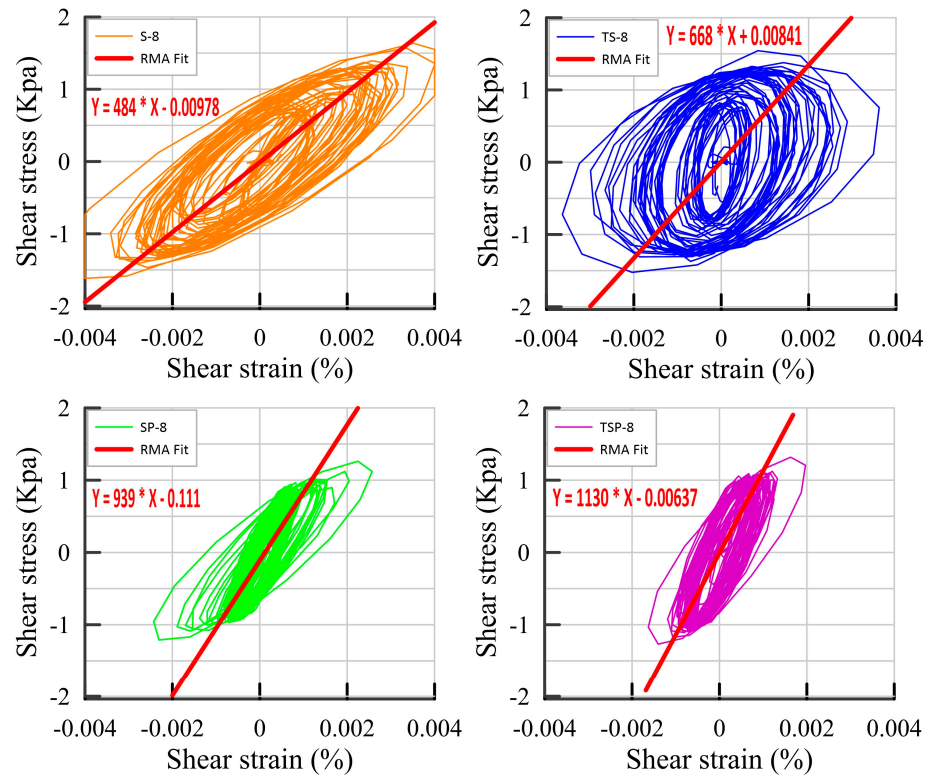


Figure 20. Shear stress–shear strain diagrams for four models at –20 cm depths at the frequency of 8 HZ.

At lower frequencies, the presence of a tunnel and a piled structure results in a reduction of strain values at the tunnel invert. The tunnel affects results more than piles

in this scenario. Conversely, above the tunnel, both the soil–pile (SP) and tunnel–soil–pile (TSP) models exhibit an increase in shear strain.

Increasing the frequency alters the model performance, resulting in higher strain values below the tunnel invert for all three models. At a depth of -35 cm, the soil–pile (SP) model reduces strains, while the tunnel–soil (TS) model dramatically increases strains. Comparing the free field soil (S) and SP models, piles improve soil profile behavior at the top, whereas the absence of piles leads to increased strain values due to reflected seismic waves at deeper depths (-55 cm). These findings emphasize the importance of incorporating piles in tunnel design to manage strain distribution.

3.3. Study of the Tunnel Lining Performance

The values of bending moments recorded in the two TS and TSP models are compared to obtain the effect of structure and piles on the bending moment values of the tunnel's section. According to Figure 3, strain gauges were installed on the outside of the tunnel.

This section includes diagrams illustrating the additional strain and bending moment induced by each loading process. It should be noted that before applying dynamic loads, static load-induced strain and bending moment were present due to the weight of the soil. However, these initial values are omitted from the results, and the presented values solely show the strain and bending moment generated by dynamic loading. Strain gauges provide negative values to indicate a reduction in concavity and positive values to indicate an increase in concavity within the tunnel section. In other words, negative bending moments correspond to an increase in the radius of curvature, whereas positive bending moments indicate a decrease in the section's curvature radius. Figure 21 shows the bending moment values obtained from the TS-3 and TSP-3 tests for strain gauges 1 to 5. The graphs of the strain gauges show either an upward or downward trend, as observed in strain gauges 1, 3, and 5. Alternatively, some strain gauges display a fluctuating trend around the axis. It is worth noting that even after the loading, residual strain remains on the tunnel cross-section.

Analyzing the diagram for the first strain gauge (SG-1) located in the tunnel crown (Figure 21), the bending moment values are positive in the TS model, reaching a maximum value of 390 N·mm. Moreover, a residual bending moment of 180 N·mm persists in the tunnel cross-section. In contrast, the TSP test showcases a change in the bending moment sign, with the extreme point of the curve shifting to -510 N·mm. Considering the absolute value of the bending moment, which plays a crucial role in tunnel lining design, it is evident that the generated bending moment increased by 31%. The TSP model exhibits a residual bending moment of 210 (N·mm). Figure 22 provides a schematic representation of the deformed tunnel section for the critical condition in the TS-3 test. In addition to the maximum, minimum, and residual bending moment values, Table 5 presents the corresponding values associated with the mentioned point in Figure 22. This information offers a comprehensive understanding of the tunnel section's deformation and bending moment characteristics in critical conditions. Unlike deep tunnels, which deform into a diagonal oval [41], the cross-section is deformed from a circular to a vertical oval. Figure 23 and Table 6 depict the TSP-3 test results, revealing contrasting behavior compared to the TS-3 model. The cross-section changes from a circular to a horizontal oval shape. Piled structure under 0.5 g acceleration and 3 Hz frequency significantly alters the seismic behavior and deformation of the tunnel in loose sand. The piled structure increases the absolute value of the maximum bending moment by up to 34% and the absolute value of the residual moment by up to 46% at the tunnel crown. The relative density of the soil has a notable impact on bending moment values, and deep tunnels may exhibit different responses due to different geological conditions [42].

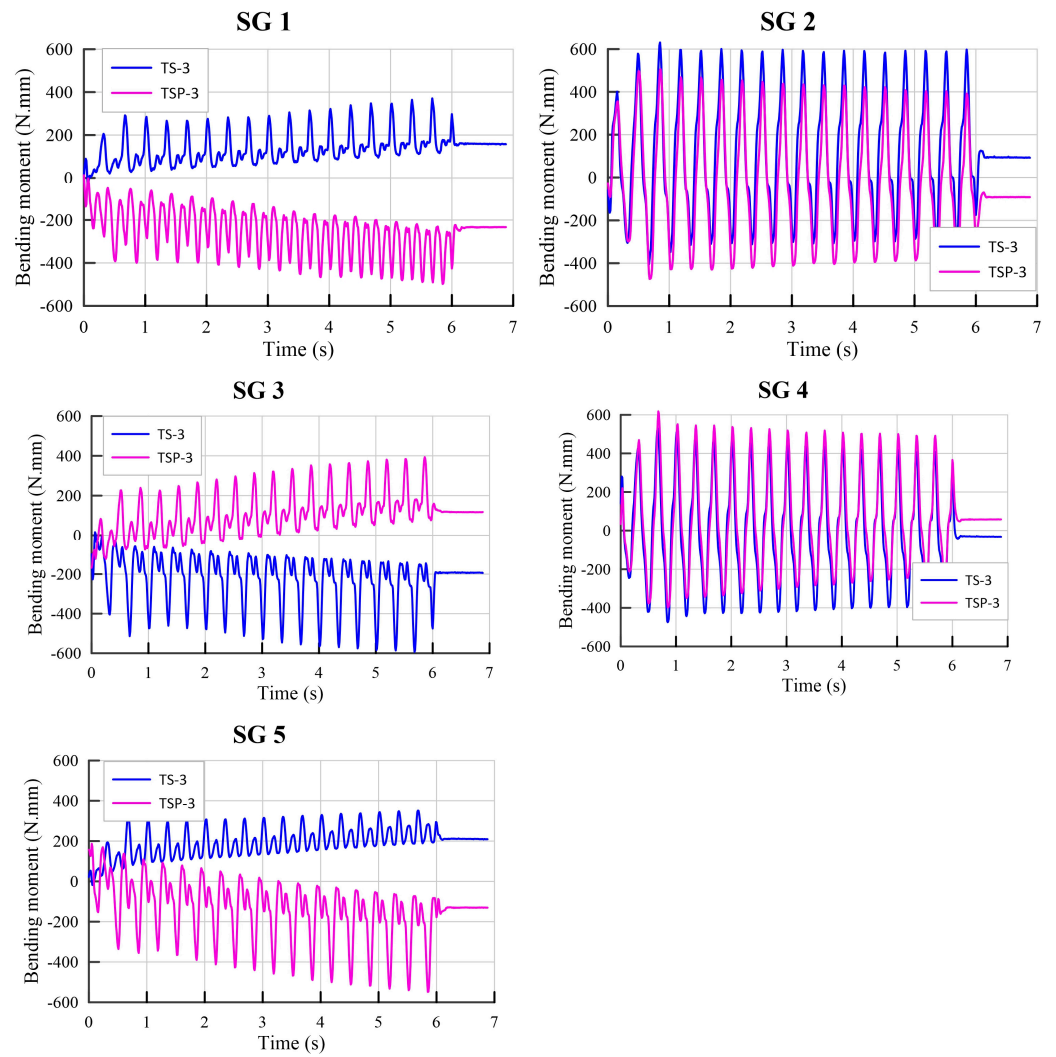


Figure 21. The bending moment values obtained for the TS-3 and TSP-3 tests for strain gauges 1–5.

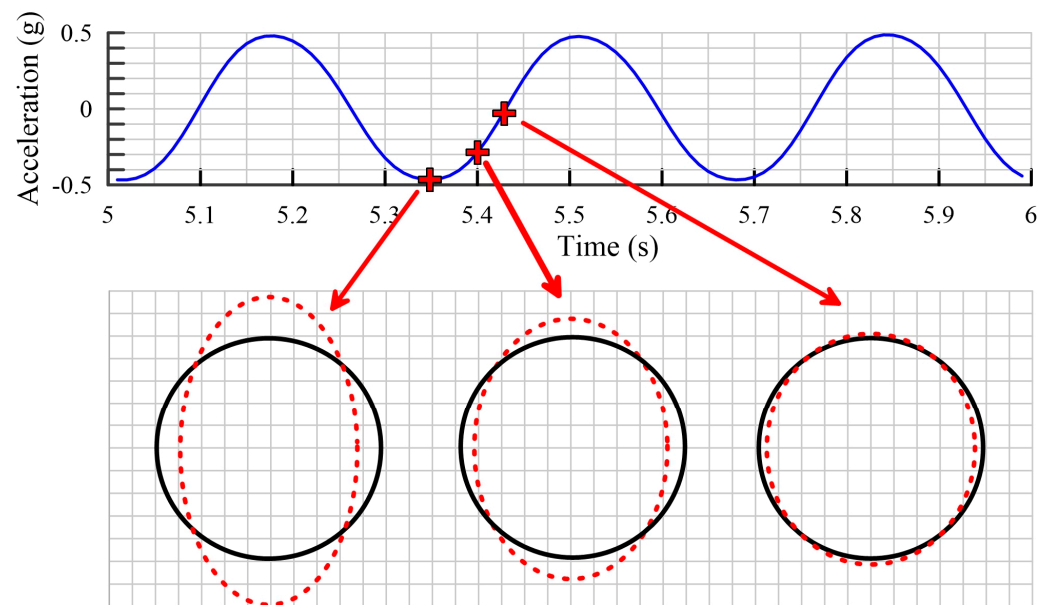


Figure 22. The schematic estimated shape of the tunnel cross-section at different moments according to the strain values for the TS-3 test.

Table 5. Bending moment values (N·mm) at the specific moments for all strain gauges for the TS-3 test.

Bending Moment (N·mm)	SG 1	SG 2	SG 3	SG 4	SG 5	SG 6	SG 7	SG 8
Time = 5.34 s	364.08	−288.24	−438.16	403.36	348.72	−197.76	−586.48	−261.12
Time = 5.38 s	221.92	−102.72	−219.52	135.12	267.92	−81.6	−304.64	−107.25
Time = 5.42 s	122.16	220	−204.16	−101.76	185.76	138.96	−144.96	241.12
Maximum	370.72	630.56	8.16	530.48	351.76	589.04	16.24	618.65
Minimum	−41.84	−404.8	−440.72	−474.8	−18.16	−382.32	−593.52	−378.9
Residual	159.44	94	−189.76	−30.08	211.12	54	−192.88	109.37

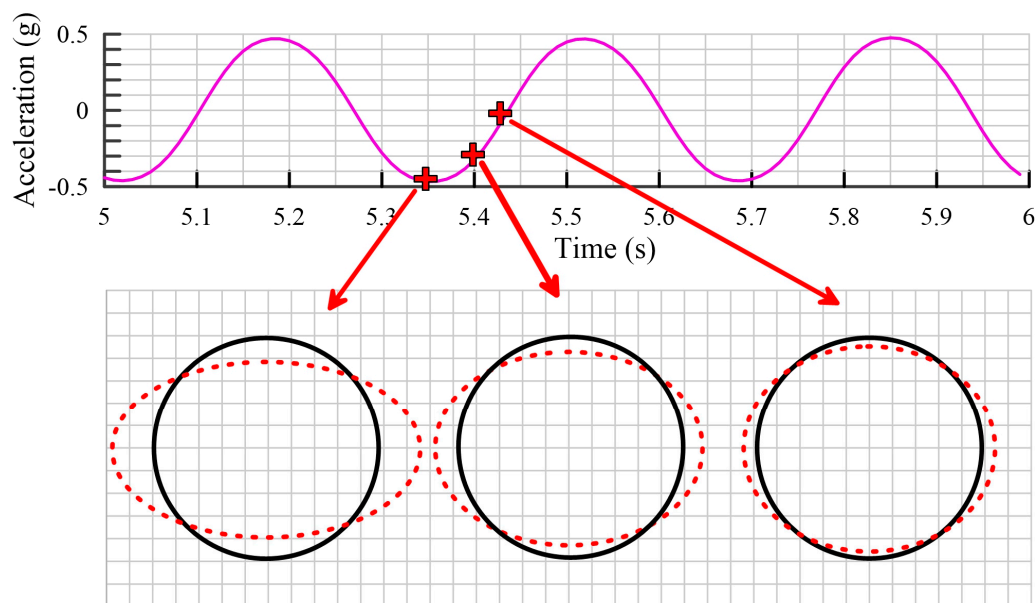


Figure 23. The schematic estimated shape of the tunnel cross-section at different moments according to the strain values for the TSP-3 test.

Table 6. Bending moment values (N·mm) at the specific moments for all strain gauges for the TSP-3 test.

Bending Moment (N·mm)	SG 1	SG 2	SG 3	SG 4	SG 5	SG 6	SG 7	SG 8
Time = 5.34 s	−472.8	−382	178.32	488.72	−209.68	−490.56	169.68	−401.2
Time = 5.38 s	−262.24	−272	140.27	226	−104.8	−326.72	157.52	−254.98
Time = 5.42 s	−227.92	−2.96	129.38	2.4	−189.12	77.6	130.72	−11.48
Maximum	12.72	505.52	421.36	618.16	186.56	561.6	393.6	438.5
Minimum	−497.92	−473.36	−154.71	−397.6	−548.64	−560.08	−168.24	−457.4
Residual	−233.36	−91.28	120.26	57.76	−130	−53.76	116.96	−67.98

In Figure 24, the deformed cross-section of the tunnel in the TS-5 experiment is displayed, and Table 7 presents the corresponding bending moment values. The behavior of this model is similar to that of the TS-3 experiment, with the cross-section transforming into a vertical oval shape under vibration. However, all bending moment values have decreased compared to the TS-3 model, with reductions of up to 73% observed in certain areas. TSP-5 model results are shown in Figure 25 and Table 8; it exhibits similar behavior to the TSP-3 model. Although the bending moment values have significantly decreased, the signs have remained unchanged.

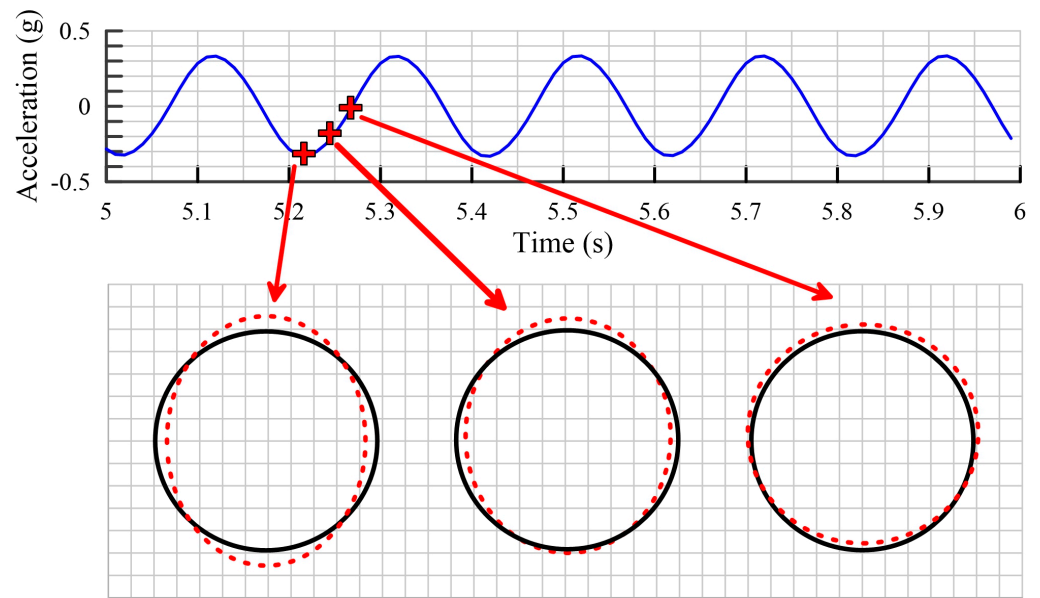


Figure 24. The schematic estimated shape of the tunnel cross-section at different moments according to the strain values for the TS-5 test.

Table 7. Bending moment values (N·mm) at the specific moments for all strain gauges for the TS-5 test.

Bending Moment (N·mm)	SG 1	SG 2	SG 3	SG 4	SG 5	SG 6	SG 7	SG 8
Time = 5.23 s	118.97	-134.86	-104.67	202.57	14.11	2.23	-109.25	-140.27
Time = 5.25 s	64.63	-82.18	-1.88	42.871	-13.41	22.34	-68.37	-70.25
Time = 5.27 s	34.94	62.364	-68.07	-14.76	-9.601	73.68	-5.248	39.75
Maximum	142.89	269.08	19.46	314.23	47.103	222.97	15.2	270.18
Minimum	-32.58	-227.55	-186.63	-125.38	-23.31	-76.42	-238.54	-248.32
Residual	58.45	-37.22	-27.65	21.63	-8.15	27.91	-30.25	-29.57

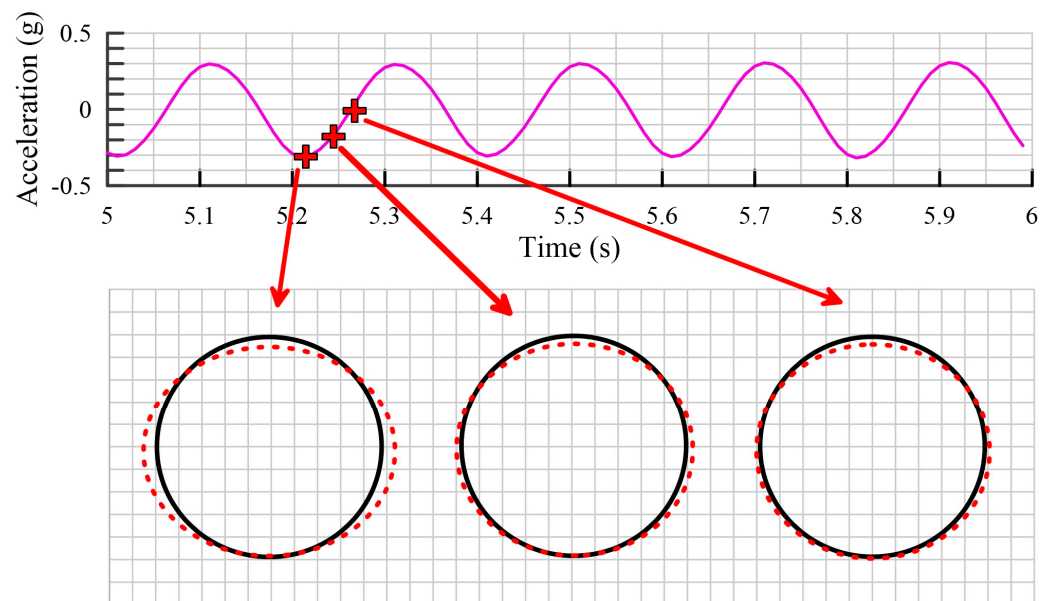


Figure 25. The schematic estimated shape of the tunnel cross-section at different moments according to the strain values for the TSP-5 test.

Table 8. Bending moment values (N·mm) at the specific moments for all strain gauges for the TSP-5 test.

Bending Moment (N·mm)	SG 1	SG 2	SG 3	SG 4	SG 5	SG 6	SG 7	SG 8
Time = 5.23 s	−73.83	−14.72	−5.32	−46.75	34.81	−71.05	−0.90	−20.23
Time = 5.25 s	−30.21	103.83	108.35	−99.54	42.44	−12.38	114.56	111.29
Time = 5.27 s	−33.72	108.58	134.81	−113.25	32.34	1.21	123.02	128.35
Maximum	26.07	182.81	260.24	57.27	44.20	95.96	274.37	168.32
Minimum	−98.57	−316.60	−30.27	−289.24	−35.70	−260.55	−25.85	−320.8
Residual	−68.36	54.45	35.25	−55.72	28.32	−37.64	35.69	47.26

Comparing Figures 24 and 25, which correspond to the TS-5 and TSP-5 experiments, reveals that similar to the 3 Hz frequency tests, the piled structure transforms the cross-section shape of the tunnel into a horizontal oval shape at 5 Hz frequency tests. The presence of the piled structure amplifies the dynamic forces exerted on the tunnel crown. However, as the buried depth of the tunnel increases, this effect may diminish, and lateral forces assume a more influential role. Notably, the recorded bending moment values for the 8 Hz frequency are too minimal, and the observed results do not follow the aforementioned behavioral pattern. Because the maximum displacement of the shaking table at an 8 Hz frequency is approximately 2 mm, the energy generated for the forced vibration of the model is insufficient to induce significant deformations.

The main limitation of this research was scaling down. Due to limited resources, a scaling factor of 45 was chosen, although it would have been better if it were less than 25. Additionally, constructing a separate tunnel model with a thinner tunnel lining for each test could have demonstrated more information about tunnel deformation and the deformed shape of the tunnel and would have helped with future designs. However, it was not possible to do so due to financial and construction limitations.

4. Conclusions

This study investigated the seismic response of shallow tunnels in a tunnel–soil–piled structure interaction system via shaking table tests conducted on loose sand. For this purpose, structure and tunnel models were designed, built, and subjected to four types of physical modeling tests using a shaking table and laminar box. Five accelerometers were embedded in the soil at various depths to examine soil response, and eight strain gauges were affixed to the tunnel model to record tunnel cross-section deformation. The results of the tests provide insights into the system’s response under seismic excitation and shed light on the influence of various factors, including the presence of a tunnel and piled structure under different excitation frequencies.

The presence of a tunnel in loose sand affects the dynamic response of the surrounding soil, and acceleration amplitude is decreased by 23% at the tunnel invert and is increased by 15% at the tunnel crown. Displacements are notably higher than the free field test at the tunnel crown, indicating the tunnel’s impact on soil deformation. It can influence the seismic response of buried structures near the tunnel, like underground stations.

At low-frequency excitation, the structure and piles near the tunnel do not significantly change the behavior of the surrounding soil. The recorded acceleration values at the tunnel invert are lower than predicted by the free-field soil model. However, as the excitation frequency increases, the acceleration values at the tunnel invert show a noticeable increase of up to 20%, indicating a stronger dynamic response. At various depths above the tunnel, there is a significant increase in acceleration, with the most notable accelerations observed in the tunnel–soil–pile model.

Based on the analysis of hysteresis curves, it becomes evident that the highest shear strain within the soil is predominantly localized in the vicinity of the tunnel’s crown. This implies that any structures in close proximity, including other tunnels and stations, must

consider this area as a critical zone in their design and safety considerations. This emphasizes the overarching necessity for the incorporation of appropriate design measures, which should not only encompass structural stability but also address the dynamic responses induced by seismic forces.

In the tunnel–soil model, the tunnel cross-section experiences significant excess bending moments, causing it to periodically change from a circular shape to a vertical oval shape. This indicates the presence of higher forces from both sides. Also, increasing the frequency leads to a notable reduction in bending moments. On the other hand, in the tunnel–soil–pile model, the tunnel cross-section changes periodically from a circular shape to a horizontal oval shape, suggesting more significant forces on the tunnel crown. Bending moments also decreased with increasing frequency. These findings highlight the distinctive behavior of shallow tunnel linings in loose sand, particularly compared to tunnels in dense sand and deeper depth. It emphasizes the importance of considering these factors in the design and analysis of shallow tunnel structures.

Dynamic loading in both the tunnel–soil and tunnel–soil–pile models generates residual bending moments within the tunnel section. The applied frequency notably influences the magnitude of these residual bending moments. Strain gauges placed at angles of 0, 90, 180, and 270 degrees of the tunnel cross-section (gauges 1, 3, 5, and 7) record the highest values of residual bending moment after the loading process.

Recommendation: Due to the close proximity of the piles and tunnel, the presence of the tunnel can influence the response of the piles, which was not explored in this study. For future research, it is suggested that the effects of existing tunnels on pile bending moments and shear strain be investigated. Additionally, a thorough examination of predicting potential scenarios for tunnel lining cracks using numerical methods and artificial intelligence is strongly recommended.

Author Contributions: Conceptualization, M.H.B.; methodology, S.E. and S.G.; software, S.E. and S.G.; validation, M.H.B. and R.D.; formal analysis, S.E. and S.G.; investigation, S.E. and S.G.; resources, M.H.B. and R.D.; data curation, S.E.; writing—original draft preparation, S.E. and S.G.; writing—review and editing, M.H.B. and R.D.; supervision, M.H.B.; funding acquisition, M.H.B. and R.D. All authors have read and agreed to the published version of the manuscript.

Funding: This research received no external funding.

Data Availability Statement: The data presented in this study are available in the article.

Conflicts of Interest: The authors declare no conflict of interest.

References

1. Yoshida, N.; Nakamura, S. Damage to Daikai Subway Station during the 1995 Hyogoken-Nunbu Earthquake and Its Investigation. In Proceedings of the Eleventh World Conference on Earthquake Engineering, Acapulco, Mexico, 23–28 June 1996.
2. Wang, Z.Z.; Jiang, Y.J.; Zhu, C.A.; Sun, T.C. Shaking Table Tests of Tunnel Linings in Progressive States of Damage. *Tunn. Undergr. Space Technol.* **2015**, *50*, 109–117. [[CrossRef](#)]
3. Xin, C.L.; Wang, Z.Z.; Gao, B. Shaking Table Tests on Seismic Response and Damage Mode of Tunnel Linings in Diverse Tunnel-Void Interaction States. *Tunn. Undergr. Space Technol.* **2018**, *77*, 295–304. [[CrossRef](#)]
4. Lu, C.C.; Hwang, J.H. Nonlinear Collapse Simulation of Daikai Subway in the 1995 Kobe Earthquake: Necessity of Dynamic Analysis for a Shallow Tunnel. *Tunn. Undergr. Space Technol.* **2019**, *87*, 78–90. [[CrossRef](#)]
5. Liu, Q. Mutual Influencing Analysis of Seismic Response of Underground and above Ground Frame Structures. In Proceedings of the 2011 International Conference on Transportation, Mechanical, and Electrical Engineering, TMEE 2011, Changchun, China, 16–18 December 2011.
6. Dowding, C.H.; Rozan, A. Damage to Rock Tunnels from Earthquake Shaking. *J. Geotech. Eng. Div.* **1978**, *104*, 175–191. [[CrossRef](#)]
7. Hashash, Y.M.A.; Hook, J.J.; Schmidt, B.; I-Chiang Yao, J. Seismic Design and Analysis of Underground Structures. *Tunn. Undergr. Space Technol.* **2001**, *16*, 247–293. [[CrossRef](#)]
8. Yu, H.; Yuan, Y.; Bobet, A. Seismic Analysis of Long Tunnels: A Review of Simplified and Unified Methods. *Undergr. Space* **2017**, *2*, 73–87. [[CrossRef](#)]
9. Shen, Y.; Zhang, D.; Wang, R.; Li, J.; Huang, Z. SBD-K-medoids-based long-term settlement analysis of shield tunnel. *Transp. Geotech.* **2023**, *42*, 101053. [[CrossRef](#)]

10. Xu, C.; Dou, P.; Du, X.; El Naggar, M.H.; Miyajima, M.; Chen, S. Large Shaking Table Tests of Pile-Supported Structures in Different Ground Conditions. *Soil Dyn. Earthq. Eng.* **2020**, *139*, 106307. [[CrossRef](#)]
11. Durante, M.G.; Di Sarno, L.; Mylonakis, G.; Taylor, C.A.; Simonelli, A.L. Soil-Pile-Structure Interaction: Experimental Outcomes from Shaking Table Tests. *Earthq. Eng. Struct. Dyn.* **2016**, *45*, 1041–1061. [[CrossRef](#)]
12. Lombardi, D.; Bhattacharya, S. Evaluation of Seismic Performance of Pile-Supported Models in Liquefiable Soils. *Earthq. Eng. Struct. Dyn.* **2016**, *45*, 1019–1038. [[CrossRef](#)]
13. Lombardi, D.; Bhattacharya, S. Modal Analysis of Pile-Supported Structures during Seismic Liquefaction. *Earthq. Eng. Struct. Dyn.* **2014**, *43*, 119–138. [[CrossRef](#)]
14. Goel, R.K.; Chopra, A.K. Period Formulas for Concrete Shear Wall Buildings. *J. Struct. Eng.* **1998**, *124*, 426–433. [[CrossRef](#)]
15. Mylonakis, G.; Gazetas, G. Seismic Soil-Structure Interaction: Beneficial or Detrimental? *J. Earthq. Eng.* **2000**, *4*, 277–301. [[CrossRef](#)]
16. Khalil, L.; Sadek, M.; Shahrour, I. Influence of the Soil-Structure Interaction on the Fundamental Period of Buildings. *Earthq. Eng. Struct. Dyn.* **2007**, *36*, 2445–2453. [[CrossRef](#)]
17. Crowley, H.; Pinho, R. Revisiting Eurocode 8 Formulae for Periods of Vibration and Their Employment in Linear Seismic Analysis. *Earthq. Eng. Struct. Dyn.* **2010**, *39*, 223–235. [[CrossRef](#)]
18. Jongpradist, P.; Kaewsri, T.; Sawatparnich, A.; Suwansawat, S.; Youwai, S.; Kongkitkul, W.; Sunitsakul, J. Development of Tunneling Influence Zones for Adjacent Pile Foundations by Numerical Analyses. *Tunn. Undergr. Space Technol.* **2013**, *34*, 96–109. [[CrossRef](#)]
19. Ptilakis, K.; Tsinidis, G.; Leanza, A.; Maugeri, M. Seismic Behaviour of Circular Tunnels Accounting for above Ground Structures Interaction Effects. *Soil Dyn. Earthq. Eng.* **2014**, *67*, 1–15. [[CrossRef](#)]
20. Azadi, M.; Hosseini, S.M.M.M. The Impact of Underground Tunnel Excavation on Adjacent Buildings during Earthquake; Case Study: Shiraz Underground, Iran. *Electron. J. Geotech. Eng.* **2007**, *12*, 1–10.
21. Wang, G.; Yuan, M.; Miao, Y.; Wu, J.; Wang, Y. Experimental Study on Seismic Response of Underground Tunnel-Soil-Surface Structure Interaction System. *Tunn. Undergr. Space Technol.* **2018**, *76*, 145–159. [[CrossRef](#)]
22. Franza, A.; Marshall, A.M.; Haji, T.; Abdelatif, A.O.; Carbonari, S.; Morici, M. A Simplified Elastic Analysis of Tunnel-Piled Structure Interaction. *Tunn. Undergr. Space Technol.* **2017**, *61*, 104–121. [[CrossRef](#)]
23. Ahn, S.; Park, G.; Yoon, H.; Han, J.-H.; Jung, J. Evaluation of Soil-Structure Interaction in Structure Models via Shaking Table Test. *Sustainability* **2021**, *13*, 4995. [[CrossRef](#)]
24. Yuan, Q.; Xiao, M.; Kong, C.; Wang, K. Seismic Response and Security Assessment of Cross-Fault Hydraulic-Tunnel Lining Structures. *Buildings* **2023**, *13*, 2348. [[CrossRef](#)]
25. Nokande, S.; Jafarian, Y.; Haddad, A. Shaking Table Tests on the Liquefaction-Induced Uplift Displacement of Circular Tunnel Structure. *Undergr. Space* **2023**, *10*, 182–198. [[CrossRef](#)]
26. Liu, Y.; Zhang, Q.; Liu, W.; Wang, T.; Liang, Z.; Liu, Z.; Liu, G.; Xu, H. Model Test Study on the Response of Two Different Shallow-Foundation Framed Buildings under Tunnel Volume Loss. *Buildings* **2023**, *13*, 2270. [[CrossRef](#)]
27. Sohaei, H.; Namazi, E.; Hajihassani, M.; Marto, A. A Review on Tunnel–Pile Interaction Applied by Physical Modeling. *Geotech. Geol. Eng.* **2020**, *38*, 3341–3362. [[CrossRef](#)]
28. Tsinidis, G.; de Silva, F.; Anastasopoulos, I.; Bilotta, E.; Bobet, A.; Hashash, Y.M.A.; He, C.; Kampas, G.; Knappett, J.; Madabhushi, G.; et al. Seismic Behaviour of Tunnels: From Experiments to Analysis. *Tunn. Undergr. Space Technol.* **2020**, *99*, 103334. [[CrossRef](#)]
29. Wang, J.; Liu, H.; Liu, H.; Zou, Y. Centrifuge Model Study on the Seismic Responses of Shield Tunnel. *Tunn. Undergr. Space Technol.* **2019**, *92*, 103036. [[CrossRef](#)]
30. Dutta, S.C.; Saha, R.; Haldar, S. Inelastic Seismic Behavior of Soil-Pile Raft-Structure System under Bi-Directional Ground Motion. *Soil Dyn. Earthq. Eng.* **2014**, *67*, 133–157. [[CrossRef](#)]
31. Bao, X.; Morikawa, Y.; Kondo, Y.; Nakamura, K.; Zhang, F. Shaking Table Test on Reinforcement Effect of Partial Ground Improvement for Group-Pile Foundation and Its Numerical Simulation. *Soils Found.* **2012**, *52*, 1043–1061. [[CrossRef](#)]
32. Iai, S. Similitude for Shaking Table Tests on Soil-Structure-Fluid Model in 1g Gravitational Field. *Soils Found.* **1989**, *29*, 105–118. [[CrossRef](#)]
33. Cao, Z.; Bai, X.; Yuan, Z.; Wang, J.; Zheng, K.; Xu, Y. An Analytical Solution for the Dynamic Tunnel–Soil–Shallow Foundation Interaction under a Harmonic Point Load. *Soil Dyn. Earthq. Eng.* **2023**, *164*, 107647. [[CrossRef](#)]
34. Ding, X.; Feng, L.; Wang, C.; Chen, Z.; Han, L. Shaking Table Tests of the Seismic Response of a Utility Tunnel with a Joint Connection. *Soil Dyn. Earthq. Eng.* **2020**, *133*, 106133. [[CrossRef](#)]
35. Yu, J.; Wang, Z.Z. The Dynamic Interaction of the Soil-Tunnel-Building System under Seismic Waves. *Soil Dyn. Earthq. Eng.* **2021**, *144*, 106686. [[CrossRef](#)]
36. Tsinidis, G. Response of Urban Single and Twin Circular Tunnels Subjected to Transversal Ground Seismic Shaking. *Tunn. Undergr. Space Technol.* **2018**, *76*, 177–193. [[CrossRef](#)]
37. Zeghal, M.; Elgamal, A.W. Analysis of Site Liquefaction Using Earthquake Records. *J. Geotech. Eng.* **1994**, *120*, 996–1017. [[CrossRef](#)]
38. Zeghal, M.; Elgamal, A.W.; Tang, H.T.; Stepp, J.C. Lotung Downhole Array. II: Evaluation of Soil Nonlinear Properties. *J. Geotech. Eng.* **1995**, *121*, 363–378. [[CrossRef](#)]
39. Roesset, J.M. Soil Amplification of Earthquakes. In *Numerical Models in Geotechnical Engineering*; McGraw-Hill: New York, NY, USA, 1977; pp. 639–682.

40. Gazetas, G. Vibrational Characteristics of Soil Deposits with Variable Wave Velocity. *Int. J. Numer. Anal. Methods Geomech.* **1982**, *6*, 1–20. [[CrossRef](#)]
41. Abdel-Motaal, M.A.; El-Nahhas, F.M.; Khiry, A.T. Mutual Seismic Interaction between Tunnels and the Surrounding Granular Soil. *HBRC J.* **2014**, *10*, 265–278. [[CrossRef](#)]
42. Sun, Q.; Dias, D. Seismic Behavior of Circular Tunnels: Influence of the Initial Stress State. *Soil Dyn. Earthq. Eng.* **2019**, *126*, 105808. [[CrossRef](#)]

Disclaimer/Publisher’s Note: The statements, opinions and data contained in all publications are solely those of the individual author(s) and contributor(s) and not of MDPI and/or the editor(s). MDPI and/or the editor(s) disclaim responsibility for any injury to people or property resulting from any ideas, methods, instructions or products referred to in the content.